

# RSC Advances



This is an *Accepted Manuscript*, which has been through the Royal Society of Chemistry peer review process and has been accepted for publication.

*Accepted Manuscripts* are published online shortly after acceptance, before technical editing, formatting and proof reading. Using this free service, authors can make their results available to the community, in citable form, before we publish the edited article. This *Accepted Manuscript* will be replaced by the edited, formatted and paginated article as soon as this is available.

You can find more information about *Accepted Manuscripts* in the [Information for Authors](#).

Please note that technical editing may introduce minor changes to the text and/or graphics, which may alter content. The journal's standard [Terms & Conditions](#) and the [Ethical guidelines](#) still apply. In no event shall the Royal Society of Chemistry be held responsible for any errors or omissions in this *Accepted Manuscript* or any consequences arising from the use of any information it contains.

# SERS performance of graphene oxide decorated silver nanoparticles/titania nanotube array

Yibing Xie<sup>a, b\*</sup>, Yujie Meng<sup>a, b</sup>

Graphene oxide (GO) decorated silver nanoparticles/titania nanotube array (Ag/TiO<sub>2</sub> NTA) had been designed as a surface-enhanced Raman scattering (SERS) substrate for a sensitive detection of organic molecules. Anatase TiO<sub>2</sub> NTA was synthesized by controlled anodic oxidation and annealing treatment processes. Ag/TiO<sub>2</sub> NTA was formed by depositing silver nanoparticles (Ag NPs) on the surface of anatase TiO<sub>2</sub> NTA through the polyol process. GO/Ag/TiO<sub>2</sub> NTA was prepared by decorating GO on the surface of Ag/TiO<sub>2</sub> NTA through an impregnation process. Methyl blue (MB) was used as the probe molecule to evaluate the adsorption capability and SERS activity of the as-prepared SERS substrates. The adsorption ratio of MB was increased from 25.2% for Ag/TiO<sub>2</sub> NTA up to 38.0% for GO/Ag/TiO<sub>2</sub> NTA, presenting an obvious improvement of the adsorption capability. The analytical enhancement factor was increased from  $1.06 \times 10^4$  for Ag/TiO<sub>2</sub> NTA up to  $3.67 \times 10^4$  for GO/Ag/TiO<sub>2</sub> NTA, presenting an obvious improvement of SERS detection performance. GO/Ag/TiO<sub>2</sub> NTA substrate accordingly achieved a very low detection limit of  $1.0 \times 10^{-9}$  M MB. GO/Ag/TiO<sub>2</sub> NTA also exhibited good adsorption capability to bisphenol A (BPA) with a weak affinity, presenting SERS detection limit of  $5 \times 10^{-7}$  M BPA. Moreover, GO/Ag/TiO<sub>2</sub> NTA was able to achieve self-cleaning function through photocatalytic degradation of organic molecule adsorbed on SERS substrate under solar light irradiation. GO/Ag/TiO<sub>2</sub> NTA having good adsorption capability, self-cleaning property, reproducibility and cycleability contributed to a promising application for sensitive and recycling SERS detection.

## 1. Introduction

Surface-enhanced Raman scattering (SERS) spectroscopy, as a quite powerful tool, has been applied in environmental monitoring, chemical analysis and biomedical research due to its supersensitivity, rapid response and fingerprint effect<sup>1-3</sup>. Two main mechanisms generally contribute to the Raman scattering enhancement observed in SERS, which involve the electromagnetic mechanism and the chemical enhancement mechanism. The former is based on the enhancement of the local electromagnetic field, whereas the latter is based on charge transfer between adsorbed molecules and metal surface<sup>4</sup>. Since the surface morphologies and structures of the substrates determine the generation and intensity of Raman signals, the substrates play a vital role in SERS detection<sup>5</sup>. An efficient SERS substrate can not only provide strong surface enhancement of Raman scattering, but also stable, reproducible and recyclable SERS detection<sup>6, 7</sup>. It is well known that the nanostructured noble metals (such as silver and gold) can be well used as SERS substrates to generate strong SERS effect<sup>8, 9</sup>. Such noble metals with well-controlled nanoarray structure can further improve the sensitivity and reproducibility of SERS detection<sup>10, 11</sup>. TiO<sub>2</sub> or TiN nanotube or nanopore arrays with well ordered and aligned nanostructure have been well fabricated as feasible supporting materials for versatile applications<sup>12-20</sup>. It has been found that TiO<sub>2</sub> can also generate weak SERS activity<sup>21</sup>. In addition, anatase TiO<sub>2</sub> has been extensively used for photocatalytic degradation of organic compounds because of its high photocatalytic activity, nontoxicity and stability<sup>22</sup>. Therefore, it is reasonable to fabricate noble metal decorated TiO<sub>2</sub> for both SERS detection and photocatalysis application. After SERS measurements, the substrates can achieve a self-cleaning function by a photocatalytic process and recycled for subsequent SERS detection<sup>23, 24</sup>.

In addition to the nanostructured noble metals, the sensitivity of SERS detection also relies on the amount of analyte molecules in the enhancement region<sup>25</sup>. In other words, SERS effect is observed when organic molecules are adsorbed on the SERS substrate. The insufficient molecule adsorption usually causes low electromagnetic enhancement and chemical enhancement effect. Therefore, SERS substrate with high adsorption capacity is essential for sensitive SERS detection. Grapheme oxide (GO) is a one-atom-thick and two dimensional carbon network containing carboxylic acid groups at the sheet edges, as well as hydroxyl and epoxy groups on the graphite plane<sup>26</sup>. Owing to the presence of aromatic domains and high specific surface area, GO is an ideal host material to adsorb a wide variety of organic molecules. Moreover, GO can chemically enhance the Raman signals of adsorbed molecules because the graphene has been recently reported to be used as a substrate with Raman enhancement effect. The observed SERS

<sup>a</sup> School of Chemistry and Chemical Engineering, Southeast University, Nanjing 211189, China, E-mail: ybxie@seu.edu.cn

<sup>b</sup> Suzhou Research Institute of Southeast University, Suzhou 215123, China

phenomenon has been ascribed to chemical enhancement mechanism<sup>27</sup>. Recently, it is reported that a noble metal/graphene oxide as SERS substrate is capable of sensitive detection of a variety of organic molecules, especially aromatic compounds keeping high affinity toward GO<sup>25</sup>. AgNPs/GO hybrid material can be applied for SERS detection, showing 2-3 times of Raman signal enhancement when compared to pure Ag NPs<sup>28</sup>. Ag NPs/reduced graphene oxide on silicon surface as the substrate can be used as an efficient SERS substrate to detect aromatic molecules with a low detection limit at scale of  $10^{-9}$  M<sup>29</sup>.

In this study, GO decorated Ag/TiO<sub>2</sub> NTA (GO/Ag/TiO<sub>2</sub> NTA) was design as a stable and recyclable SERS substrate for sensitive SERS detection of organic compounds and photocatalytic self-cleaning<sup>30</sup>. Fig. 1 shows the schematic displaying the fabrication process of GO/Ag/TiO<sub>2</sub> NTA substrate. Briefly, highly ordered anatase TiO<sub>2</sub> NTA was synthesized by a controlled anodic oxidation and annealing treatment process. The well-dispersed Ag NPs were deposited on the surface of anatase TiO<sub>2</sub> NTA to form Ag/TiO<sub>2</sub> NTA via the polyol process<sup>31</sup>. GO was then decorated on the surface of Ag/TiO<sub>2</sub> NTA to form GO/Ag/TiO<sub>2</sub> NTA through an impregnation process<sup>32</sup>. The adsorption capability and SERS activity of Ag/TiO<sub>2</sub> NTA and GO/Ag/TiO<sub>2</sub> NTA were investigated. The sensitivity and recyclability of GO/Ag/TiO<sub>2</sub> NTA were fully evaluated using methyl blue as the probe molecule. GO/Ag/TiO<sub>2</sub> NTA was also used for SERS detection of bisphenol A with a weak adsorption affinity.

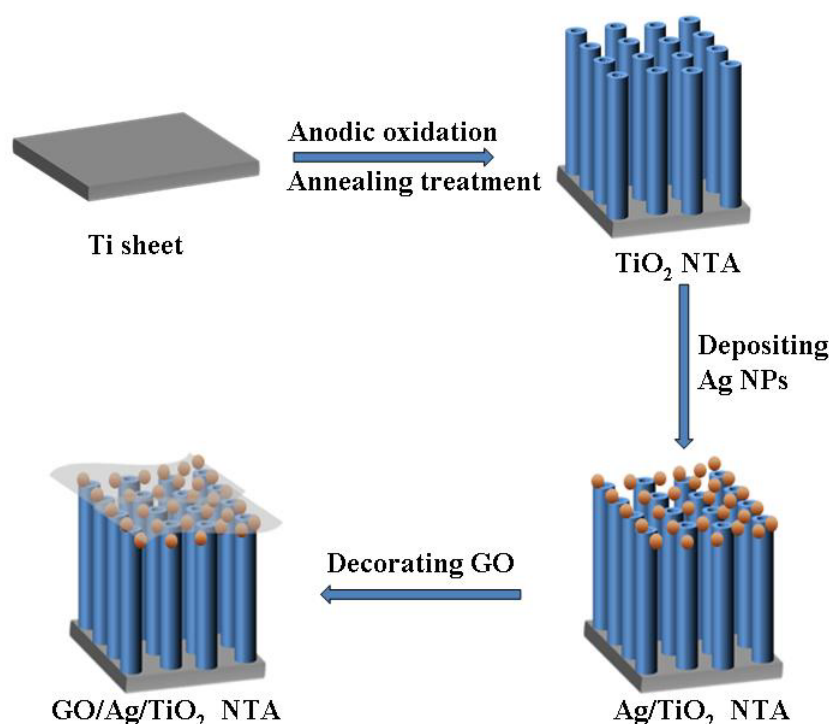


Fig. 1 Schematic displaying the fabrication process of GO/Ag/TiO<sub>2</sub> NTA substrate.

## 2. Experimental

### 2.1 Material

Titanium sheet (Ti, thickness of 0.2 mm, purity >99.6%) was purchased from Good fellow Cambridge Ltd. Ethylene glycol (EG), ammonium fluoride (NH<sub>4</sub>F), phosphoric acid (H<sub>3</sub>PO<sub>4</sub>), silver nitrate (AgNO<sub>3</sub>), sodium borohydride (NaBH<sub>4</sub>), polyvinylpyrrolidone (PVP) and methyl blue (MB) bisphenol A (BPA) and ethanol purchased from Sinopharm chemical company are analytical grade and used without further purification. Distilled water was fully used in all experiments.

### 2.2 Preparation of GO/Ag/TiO<sub>2</sub> NTA

TiO<sub>2</sub> NTA was fabricated by anodic oxidation of titanium sheet. The anodization process was conducted at 30 V for 2 h in water and ethylene glycol mixture solution (volume ratio, 1:1) containing 0.5 M H<sub>3</sub>PO<sub>4</sub> and 0.2 M NH<sub>4</sub>F in a two-electrode cell using Ti foil as the working electrode and a Pt sheet as the counter electrode. The obtained amorphous TiO<sub>2</sub> was annealed at 450°C for 2 h to form anatase TiO<sub>2</sub> NTA with photocatalytic activity. Ag/TiO<sub>2</sub> NTA was fabricated by depositing Ag NPs on the surface of TiO<sub>2</sub> NTA through the polyol process. Briefly, the as-prepared TiO<sub>2</sub> NTA was immersed in water and ethylene glycol mixture solution (volume

ratio, 1:1) containing 0.001 M PVP, 0.035 M NaBH<sub>4</sub>, 0.055 M AgNO<sub>3</sub> at ambient temperature for 7 h, and subsequently rinsed with DI water and dried in vacuum. GO was prepared through chemically oxidizing graphite powders by a modified Hummers method<sup>33</sup>. The GO/Ag/TiO<sub>2</sub> NTA was obtained by decorating GO on Ag/TiO<sub>2</sub> through an impregnation method. Typically, the as-prepared Ag/TiO<sub>2</sub> NTA was immersed in a 0.5 mg mL<sup>-1</sup> GO aqueous solution for 3 h, and subsequently rinsed with DI water and dried in vacuum. For a comparison, GO/TiO<sub>2</sub> NTA was also fabricated by coating GO on the surface of TiO<sub>2</sub> NTA using the same above method.

### 2.3 Characterization

The surface morphologies of TiO<sub>2</sub>, Ag/TiO<sub>2</sub>, and GO/Ag/TiO<sub>2</sub> NTA were characterized by the Field-Emission Scanning Electron Microscope (FE-SEM, Zeiss Ultra-Plus). UV-vis spectrum was measured to analyze MB concentration by UV/Vis Spectrometer (Shimadzu UV-2100 UV/Vis Spectrometer). Raman spectrum was measured to investigate SERS substrates using a Renishaw Invia Reflex System Raman spectrometer. The single layer structure of graphene oxide was investigated using a transmission electron microscope (TEM, JEOJ-2010) with an acceleration voltage of 200 kV. The excitation wavelength was 785 nm. The 50× objective lens was used to focus the laser light on the samples. The laser power was 1%, and integration time for each sample was 10 s.

### 2.4 Adsorption measurement

TiO<sub>2</sub>, Ag/TiO<sub>2</sub>, GO/TiO<sub>2</sub>, and GO/Ag/TiO<sub>2</sub> NTA were respectively immersed in freshly prepared 1.0×10<sup>-5</sup> M MB and 2.2×10<sup>-4</sup> M BPA solution for 2 h in the dark at ambient temperature to achieve the adsorption equilibrium. The concentration change of MB and BPA solution before and after the adsorption on different substrates was analyzed according to the of characteristic peak intensity of UV-vis spectrum.

### 2.5 SERS measurement

All SERS substrates were immersed in freshly prepared MB or BPA solution with controlled concentration for 2 h in the dark, then rinsed with solvent and dried in vacuum for the Raman spectrum measurements. The Ag/TiO<sub>2</sub>, GO/TiO<sub>2</sub> and GO/Ag/TiO<sub>2</sub> NTA were used for SERS detection of 10<sup>-5</sup> M MB solution. The GO/Ag/TiO<sub>2</sub> NTA was used for SERS detection of MB solution with different concentration from 10<sup>-9</sup> to 10<sup>-4</sup> M. The Ag/TiO<sub>2</sub> and GO/Ag/TiO<sub>2</sub> NTA were used for SERS detection of 5×10<sup>-4</sup> M BPA solution. The GO/Ag/TiO<sub>2</sub> NTA was used for SERS detection of BPA ethanol solution with different concentrations from 5×10<sup>-7</sup> M to 5×10<sup>-4</sup> M.

## 3. Results and discussion

### 3.1. Characterization of Ag/TiO<sub>2</sub> NTA and GO/Ag/TiO<sub>2</sub> NTA

Fig. 2(A-E) shows the SEM images of TiO<sub>2</sub>, Ag/TiO<sub>2</sub> NTA and GO/Ag/TiO<sub>2</sub> NTA. TiO<sub>2</sub> NTA exhibited highly ordered, vertically aligned nanotube microstructure with tube diameter of 100 - 120 nm, tube length of 850 - 950 nm and tube wall thicknesses of 15 - 20 nm. The interspace between the neighboring tubes is 40 - 60 nm. (see Fig. 2(A and B)). Concerning Ag/TiO<sub>2</sub> NTA, Ag NPs with average diameter of 10 - 15 nm were evenly distributed on the pore mouth of TiO<sub>2</sub> NTA. Such Ag NPs were hardly observed on the tube walls of TiO<sub>2</sub> NTA (see Fig. 2(C and D)). Concerning GO/Ag/TiO<sub>2</sub> NTA, a continuous and transparent GO monolayer film was well coated on the top surface of Ag/TiO<sub>2</sub> NTA (see Fig. 2(E and F)). Fig. 2G shows the TEM image of GO. Obviously, GO kept a transparent and well expanding monolayer structure. Such a GO was very suitable for functional modification of Ag NPs to achieve good adsorption capability and SERS activity as well.

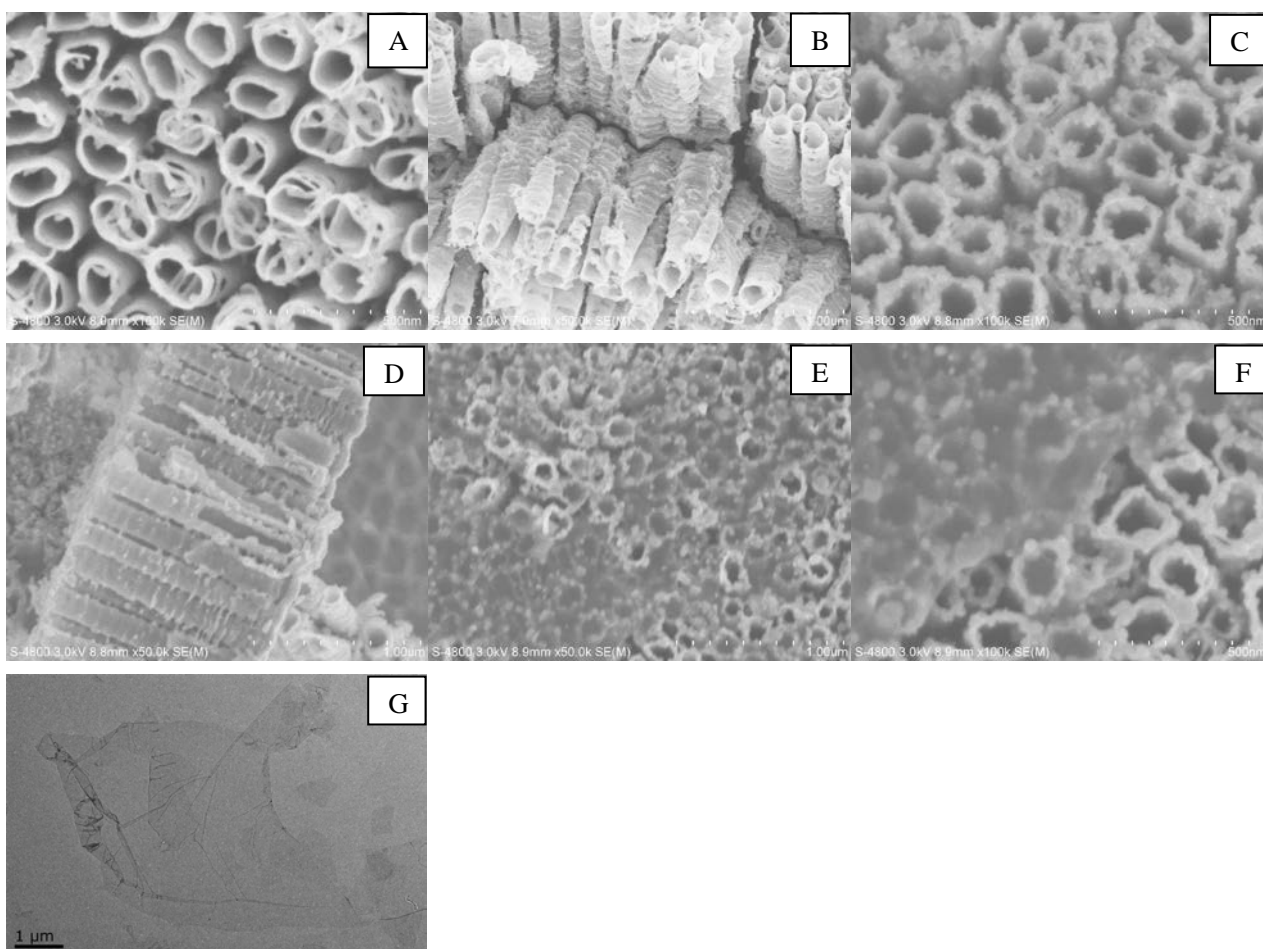


Fig. 2 SEM images of (A, B) TiO<sub>2</sub> NTA; (C, D) Ag/TiO<sub>2</sub> NTA and (E, F) GO/Ag/TiO<sub>2</sub> NTA; TEM image of GO.

Raman spectroscopy was employed to further confirm the transparent GO coating layer on the surface of Ag/TiO<sub>2</sub> NTA. Fig. 3 shows the Raman spectra of Ag/TiO<sub>2</sub> NTA and GO/Ag/TiO<sub>2</sub> NTA. The Raman characteristic peaks at 155, 396, 517, 638 cm<sup>-1</sup> were observed in both samples, which were assigned to the E<sub>g</sub>, B<sub>1g</sub>, B<sub>1g</sub> or A<sub>1g</sub>, E<sub>g</sub> modes of anatase TiO<sub>2</sub>, respectively<sup>34</sup>. For the GO/Ag/TiO<sub>2</sub> NTA, the two additional prominent peaks at 1320 cm<sup>-1</sup> and 1597 cm<sup>-1</sup> were regarded as the characteristic D band and G band of GO. The G-band appearing at around 1597 cm<sup>-1</sup> was a significant characteristic of sp<sup>2</sup> hybridized carbon, which could provide the information on the in-plane vibration of sp<sup>2</sup>-bonded carbon domains<sup>35</sup>. The D-band appearing at around 1320 cm<sup>-1</sup> revealed the presence of sp<sup>3</sup> defects within the hexagonal graphitic structure<sup>36</sup>, which was associated with the amorphous carbon, or edges that break the symmetry and selection rule<sup>37</sup>. Such characteristics demonstrate that the expanding GO sheets were really decorated on the Ag/TiO<sub>2</sub> NTA.

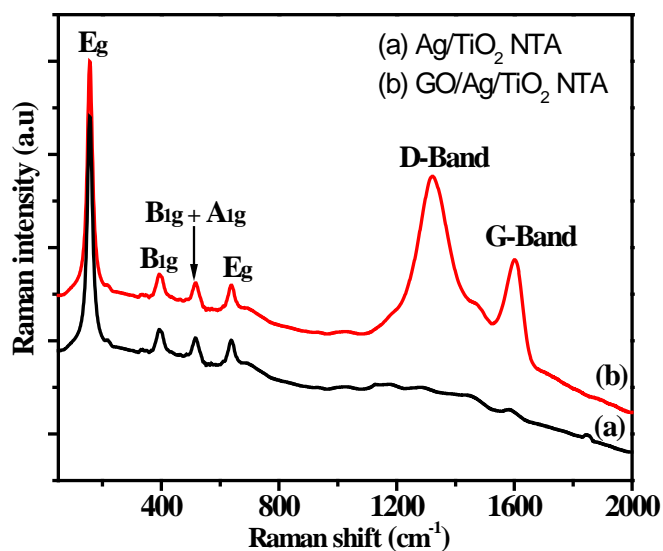
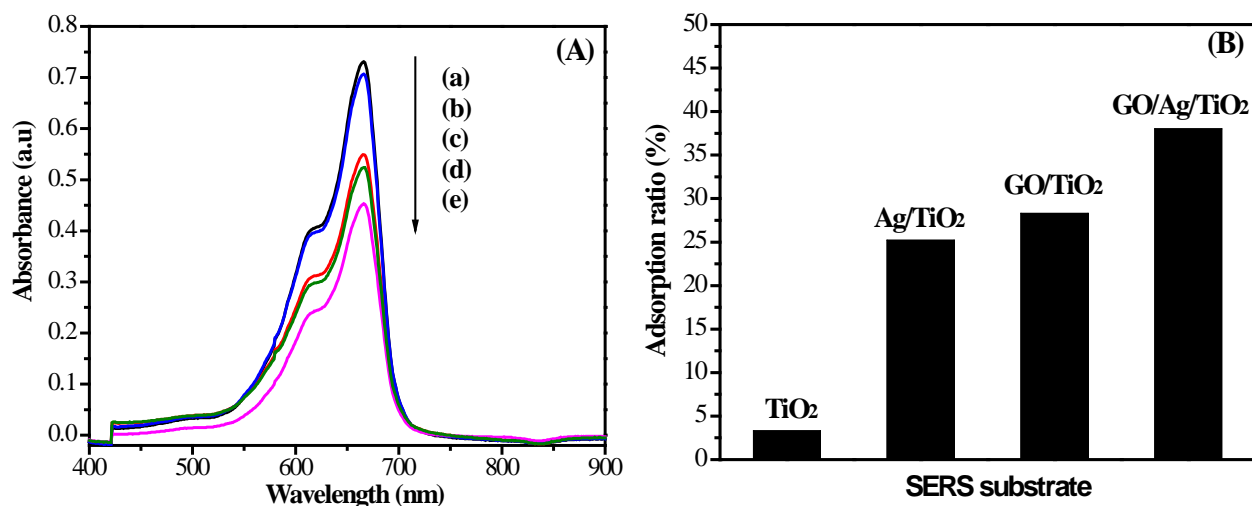


Fig. 3 Raman spectra of (a) Ag/TiO<sub>2</sub> NTA and (b) GO/Ag/TiO<sub>2</sub> NTA.

### 3.2 Adsorption capability of GO/Ag/TiO<sub>2</sub> NTA

The adsorption capability of Ag/TiO<sub>2</sub> NTA and GO/Ag/TiO<sub>2</sub> NTA were investigated by immersing these substrates in  $1.0 \times 10^{-5}$  M MB solution for 2 h in the dark. MB concentration was evaluated before and after adsorption according to the characteristic peak intensity at 664 nm using UV-Vis spectrophotometer. Fig. 4(A) shows UV-vis spectra of MB solution before and after adsorption on different SERS substrates. They demonstrated different adsorption effects. Fig. 4(B) shows the adsorption ratio of MB on different SERS substrates. The adsorption ratio of MB followed the decreasing order of GO/Ag/TiO<sub>2</sub> > GO/TiO<sub>2</sub> > Ag/TiO<sub>2</sub>. Obviously, both Ag/TiO<sub>2</sub> NTA and GO/TiO<sub>2</sub> NTA exhibited a similar adsorption capacity, but much higher than TiO<sub>2</sub> NTA. The covalent bonding between Ag NPs and MB molecule contributed to improving the adsorption capability of Ag/TiO<sub>2</sub> NTA<sup>38</sup>. Moreover, GO/Ag/TiO<sub>2</sub> NTA showed the highest adsorption capacity. This is owing to the unique chemical structure of GO. The highly negative charged GO possesses the oxygen-containing functional groups, which can interact with the positive charged MB molecule through electrostatic-interaction<sup>39</sup>. In addition, GO with aromatic domains, can also form strong  $\pi$ - $\pi$  stacking interactions with  $\pi$ -electron-rich MB molecule<sup>40</sup>. GO/Ag/TiO<sub>2</sub> NTA exhibited higher adsorption capability than GO/TiO<sub>2</sub> NTA, indicating that the introduction of Ag NPs between TiO<sub>2</sub> NTA and GO enlarged the specific surface area of the composite<sup>41</sup>.

Fig. 4(C) shows UV-vis spectra of  $2.2 \times 10^{-4}$  M BPA solution before and after adsorption on SERS substrates. The similar trend was obtained for the adsorption ratio of MB and BPA on SERS substrates. Comparatively, due to the weak adsorption affinity to the substrate, BPA exhibited weaker adsorption capability than MB. Fig. 4(D) shows the adsorption ratio of BPA on different SERS substrates. Both TiO<sub>2</sub> NTA and Ag/TiO<sub>2</sub> NTA had similar and comparable adsorption ratio of BPA, presenting low adsorption capability. This was owing to the weak affinity between Ag NPs and BPA. However, the adsorption capability of both GO/TiO<sub>2</sub> NTA and GO/Ag/TiO<sub>2</sub> NTA was much higher than that of Ag/TiO<sub>2</sub> NTA. This indicates that GO played an important role on the adsorption of BPA. The benzene rings of BPA could interact with GO through  $\pi$ - $\pi$  interaction. The hydroxyl groups of GO could form hydrogen bonds with hydroxyl groups of BPA<sup>42</sup>. These results suggest that GO/Ag/TiO<sub>2</sub> NTA indeed exhibited higher adsorption capability.



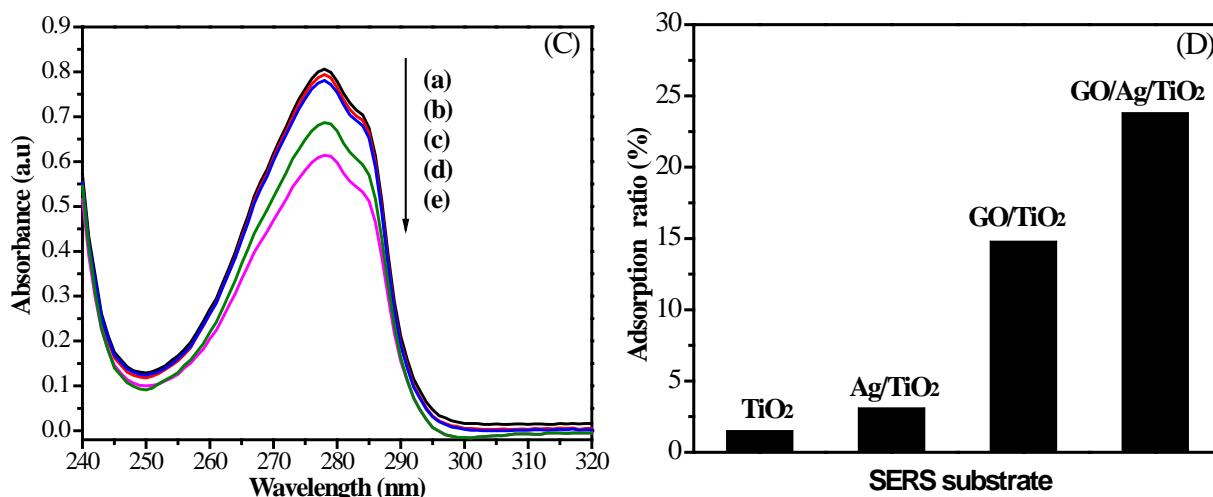


Fig. 4 UV-vis spectra and adsorption ratio of (A, B)  $10^{-5}$  M MB solution and (C, D)  $2.2 \times 10^{-4}$  M BPA solution on the substrate of TiO<sub>2</sub> NTA, Ag/TiO<sub>2</sub> NTA, GO/TiO<sub>2</sub> NTA and GO/Ag/TiO<sub>2</sub> NTA.

### 3.3 SERS performance of Ag/TiO<sub>2</sub> NTA and GO/Ag/TiO<sub>2</sub> NTA

The SERS activity of the Ag/TiO<sub>2</sub> NTA and GO/Ag/TiO<sub>2</sub> NTA was evaluated using MB as probe molecule. Fig. 5(A) shows the SERS spectra of  $10^{-5}$  M MB aqueous solution adsorbed on Ag/TiO<sub>2</sub>, GO/TiO<sub>2</sub> and GO/Ag/TiO<sub>2</sub> NTA. Obviously, SERS signals of MB molecule on all SERS substrates were observed and the characteristic bands could be clearly distinguished. The Raman peaks at  $1622 \text{ cm}^{-1}$  and  $1397 \text{ cm}^{-1}$  were corresponding to the C-C ring stretching vibration and C-N-C skeletal bending vibration of MB molecule, respectively<sup>43</sup>. Concerning GO/Ag/TiO<sub>2</sub> NTA and GO/TiO<sub>2</sub> NTA, the additional prominent peak at  $1320 \text{ cm}^{-1}$  was the characteristic D band of GO. On the other hand, the G band overlapped significantly with the C-C ring stretching vibration of MB molecule at  $1622 \text{ cm}^{-1}$ , making it difficult to distinguish above two vibration modes from each other. The SERS peak intensity obtained on the GO/Ag/TiO<sub>2</sub> NTA and Ag/TiO<sub>2</sub> NTA were far higher than that on GO/TiO<sub>2</sub> NTA. This indicates that the SERS chemical enhancement effect of GO was much weaker than SERS electromagnetic field enhancement effect of Ag NPs. The SERS peak intensity at  $1622 \text{ cm}^{-1}$  obtained on the GO/TiO<sub>2</sub> NTA was only 3.6% of that on GO/Ag/TiO<sub>2</sub> NTA. The contribution of GO layer to the Raman intensity of  $1622 \text{ cm}^{-1}$  was so small that it could be ignored in the calculation of SERS enhancement factor. Moreover, GO/Ag/TiO<sub>2</sub> NTA had better SERS performance than Ag/TiO<sub>2</sub> NTA. Firstly, it is reported that graphene coating layer did not alter the plasmonic properties of Ag NPs, causing less influence on its electromagnetic SERS enhancement<sup>44</sup>. Therefore, the ultrathin GO layer coating on the Ag NPs did not impede SERS enhancement of Ag NPs<sup>45</sup>. Secondly, GO was regarded as a favorable SERS platform. When MB was adsorbed on GO, the charge transfer process occurred between the oxygen-functional groups and MB molecule, which was the dominant mechanism contributing to the additional SERS enhancement. It was reported that the Raman peak intensity of the probe molecules descended along with the increase of the reduction degree of GO when GO was converted to reduced graphene oxide (RGO)<sup>46</sup>. The chemical enhancement of SERS using GO would arise from  $\pi$ - $\pi$  stacking and charge transfer from the oxygen-functional groups to the probe molecules. When GO was fully converted to RGO, the number of the oxygen-functional groups highly decreased, resulting in a corresponding decrease of the Raman peak intensity of the probe molecules<sup>28</sup>. Thirdly, GO had a double-sided polyaromatic scaffold with an ultrahigh specific surface area and therefore was capable of adsorbing a larger number of MB molecule. The improved adsorption of MB molecule on GO occurred in the SERS enhancement region, leading to better SERS enhancement effect<sup>25</sup>.

The enhancement effect of SERS substrates was estimated by calculating enhancement factor (EF) and analytical enhancement factor (AEF) using the equations of  $EF = (I_{\text{SERS}}/N_{\text{surface}})/(I_{\text{RS}}/N_{\text{bulk}})$  and  $AEF = (I_{\text{SERS}}/C_{\text{SERS}})/(I_{\text{RS}}/C_{\text{RS}})$ <sup>47</sup>. Herein,  $I_{\text{SERS}}$  and  $I_{\text{RS}}$  are the intensities of SERS signal and normal Raman signal at  $1622 \text{ cm}^{-1}$ ;  $C_{\text{RS}}$  and  $C_{\text{SERS}}$  are MB concentration under normal Raman and SERS condition;  $N_{\text{bulk}}$  and  $N_{\text{surface}}$  are MB molecule number illuminated by the laser focus spot under normal Raman and SERS condition. The adsorption quantity per unit area can be calculated using the equation of  $Q_e = [(C_0 - C_e) \cdot V]/S$ , where  $C_0$  and  $C_e$  are MB concentration before and after adsorption by Ag/TiO<sub>2</sub> NTA or GO/Ag/TiO<sub>2</sub> NTA;  $V$  is the volume of MB solution;  $S$  is the surface area of Ag/TiO<sub>2</sub> NTA or GO/Ag/TiO<sub>2</sub> NTA. The  $C_0$  was determined to be  $10^{-5}$  M.  $C_e$  was calculated according to the absorbance

change before and after adsorption and Lambert-Beer Law. The laser spot has a diameter of 1.0  $\mu\text{m}$  and surface area of about  $7.9 \times 10^{-9} \text{ cm}^2$ . The volume of laser focus spot is  $7.9 \times 10^{-10} \text{ L}$ . Fig. 5 shows SERS spectra of  $10^{-5} \text{ M}$  MB on Ag/TiO<sub>2</sub> NTA, GO/Ag/TiO<sub>2</sub> NTA and normal Raman spectra of  $10^{-2} \text{ M}$  MB. The MB concentration was determined to be  $10^{-5} \text{ M}$  for  $C_{\text{SERS}}$  and  $10^{-2} \text{ M}$  for  $C_{\text{RS}}$ . The adsorption quantity per unit area was estimated to be  $1.0 \text{ nmol cm}^{-2}$  for Ag/TiO<sub>2</sub> NTA and  $1.8 \text{ nmol cm}^{-2}$  for GO/Ag/TiO<sub>2</sub> NTA.  $N_{\text{surface}}$  was accordingly calculated to be  $4.8 \times 10^6$  and  $8.5 \times 10^6$ .  $N_{\text{bulk}}$  was calculated to be  $4.8 \times 10^{12}$ . As a result, the EF values of Ag/TiO<sub>2</sub> NTA and GO/Ag/TiO<sub>2</sub> NTA were estimated to be  $1.0 \times 10^7$  and  $2.1 \times 10^7$ . The corresponding AEF values were estimated to be  $1.06 \times 10^4$  and  $3.67 \times 10^4$ . For a comparison, the Raman peak at  $1397 \text{ cm}^{-1}$  was also used for the enhancement factor calculation because it was free from potential signal interference that may arise from GO. On the base of Raman peak at  $1397 \text{ cm}^{-1}$ , the EF values of Ag/TiO<sub>2</sub> NTA and GO/Ag/TiO<sub>2</sub> NTA were estimated to be  $2.2 \times 10^7$  and  $3.6 \times 10^7$ . The corresponding AEF values were estimated to be  $2.2 \times 10^4$  and  $6.4 \times 10^4$ . Similar results of the enhancement factor were obtained according to the different Raman peaks at 1622 and  $1397 \text{ cm}^{-1}$ . The Raman signal of MB was enhanced about 2-3 times using GO/Ag/TiO<sub>2</sub> NTA instead of Ag/TiO<sub>2</sub> NTA, indicating an improved SERS enhancement effect. It was also reported that GO coated on Ag octahedron was used as SERS substrate for 4-aminothiophenol detection and the EF value of GO/Ag substrate was about  $10^6$ <sup>28</sup>. The SERS activity of GO/Ag/TiO<sub>2</sub> NTA substrate was comparable with or even superior to as-reported GO/Ag substrate.

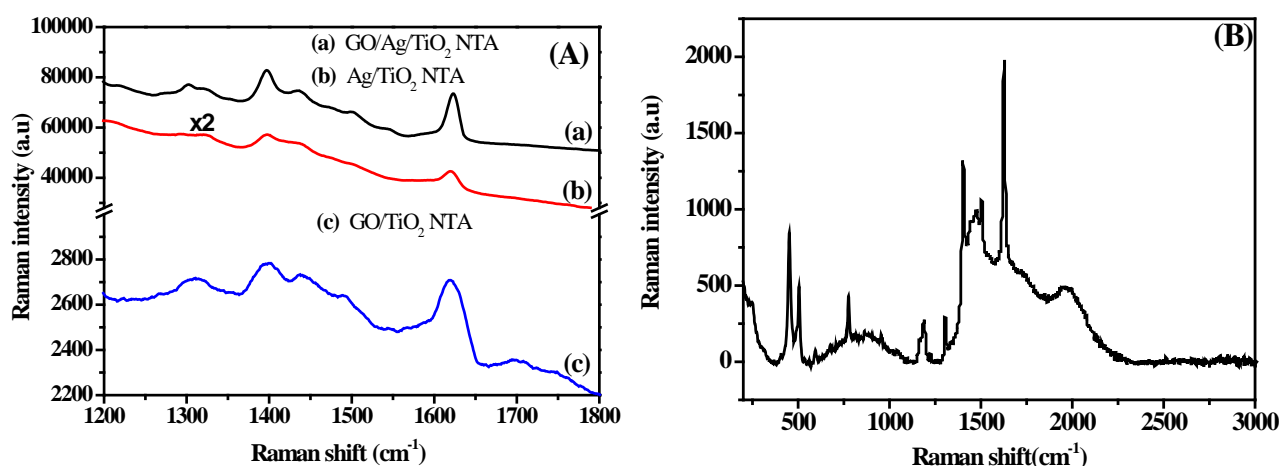


Fig. 5 (A) SERS spectra of  $10^{-5} \text{ M}$  MB aqueous solution adsorbed on (a) GO/Ag/TiO<sub>2</sub> NTA, (b) Ag/TiO<sub>2</sub> NTA and (c) GO/TiO<sub>2</sub> NTA; (B) Normal Raman spectra of  $10^{-2} \text{ M}$  MB aqueous solution.

### 3.4 SERS performance of GO/Ag/TiO<sub>2</sub> NTA

The Raman enhancement effect of GO/Ag/TiO<sub>2</sub> NTA was further investigated through SERS detection of MB solution with different concentration. Fig. 6(A) shows the Raman spectra of  $10^{-9} \text{ M}$  to  $10^{-4} \text{ M}$  MB solution adsorbed on GO/Ag/TiO<sub>2</sub> NTA substrate. The Raman characteristic peak intensity at  $1622 \text{ cm}^{-1}$  was quite sensitive to MB concentration. The corresponding Raman peak intensity descended along with the decrease of MB concentration. Fig. 6(B) shows the Raman characteristic peak intensity at  $1622 \text{ cm}^{-1}$  in terms of MB concentration. A quasi-linear relationship was determined at a low concentration range from  $10^{-9}$  to  $10^{-6} \text{ M}$ . It indicates that the SERS active sites were enough for the full adsorption of MB in this concentration range. However, such an increase of Raman peak intensity would become insignificant at the higher concentration above  $10^{-5} \text{ M}$  due to the saturated coverage of SERS active sites. The Raman signals of MB could still clearly be observed at a concentration as low as  $10^{-9} \text{ M}$ . The low detection limit at a scale of  $10^{-9} \text{ M}$  demonstrated the high sensitivity of SERS detection performance using GO/Ag/TiO<sub>2</sub> NTA substrate. The similar result with a detection limit of  $10^{-9} \text{ M}$  was also reported when using Ag NPs-decorated single-layer reduced graphene oxide film on silicon surface as the substrate for Raman spectrum detection of MB<sup>29</sup>.

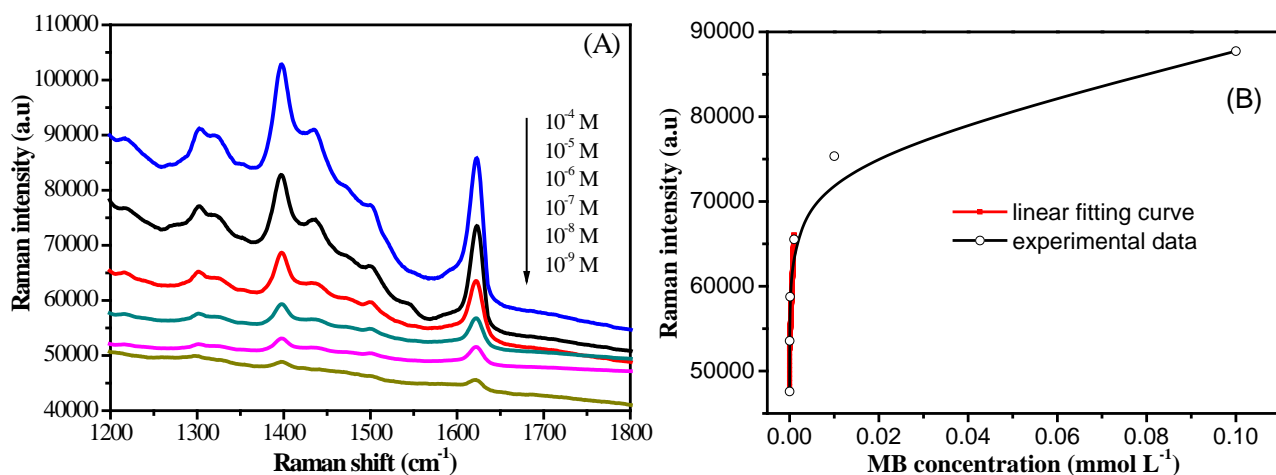


Fig. 6 (A) Raman spectra of  $10^{-9}$  M to  $10^{-4}$  M MB adsorbed on GO/Ag/TiO<sub>2</sub> NTA; (B) The intensity of Raman characteristic peaks at 1622 cm<sup>-1</sup> in terms of MB concentration.

### 3.5 Stability of GO/Ag/TiO<sub>2</sub> NTA

The stability of Ag/TiO<sub>2</sub> NTA and GO/Ag/TiO<sub>2</sub> NTA substrates were investigated through exposure treatment under ambient condition. Fig. 7 shows Raman spectra of  $10^{-4}$  M MB solution adsorbed on Ag/TiO<sub>2</sub> NTA and GO/Ag/TiO<sub>2</sub> NTA with exposure treatment for 0 day and 60 days. Concerning freshly prepared Ag/TiO<sub>2</sub> NTA and GO/Ag/TiO<sub>2</sub> NTA substrates, the Raman characteristic peaks of MB at 1622 cm<sup>-1</sup> and 1397 cm<sup>-1</sup> could be clearly detected. In view of the same substrates with exposure treatment for 60 days, The Raman characteristic peak intensity at 1622 cm<sup>-1</sup> decreased 55% for Ag/TiO<sub>2</sub> NTA and only 5% for GO/Ag/TiO<sub>2</sub> NTA. It indicates that the GO coating on the Ag NPs surface indeed could enhance the stability of Ag/TiO<sub>2</sub> NTA substrate and maintained comparable detection sensitivity. It is well known that Ag NPs are easily oxidized when exposed to ambient condition. The oxidation of the Ag NPs results in significant changes of plasmonic properties and thus will greatly affect their SERS performance<sup>48</sup>. Besides, the photobleaching phenomenon raised from the decomposition or carbonization of the organic molecules can cause a significant decrease of the SERS activity<sup>49</sup>. Concerning GO/Ag/TiO<sub>2</sub> NTA substrate, the highly impermeable GO serves as a barrier isolates Ag NPs from the oxygen in ambient environment. The GO coating layer on Ag NPs is able to prevent Ag NPs from oxidation. Meanwhile, the GO also stabilizes the probe molecule via  $\pi$ - $\pi$  interaction. This interaction enables the charge transfer between GO and MB molecule. MB molecule can be excited from ground state to excitation state when absorbing suitable photon energy. The GO in the GO/Ag/TiO<sub>2</sub> NTA provides additional path for the MB molecule to relax from excitation state to ground state, avoiding the probability of photobleaching phenomenon<sup>50</sup>.

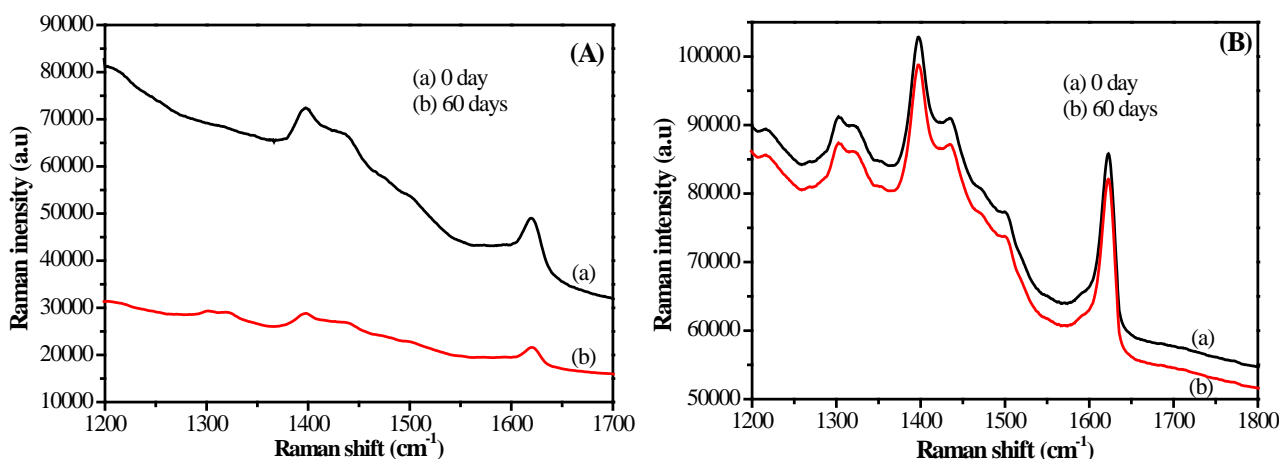
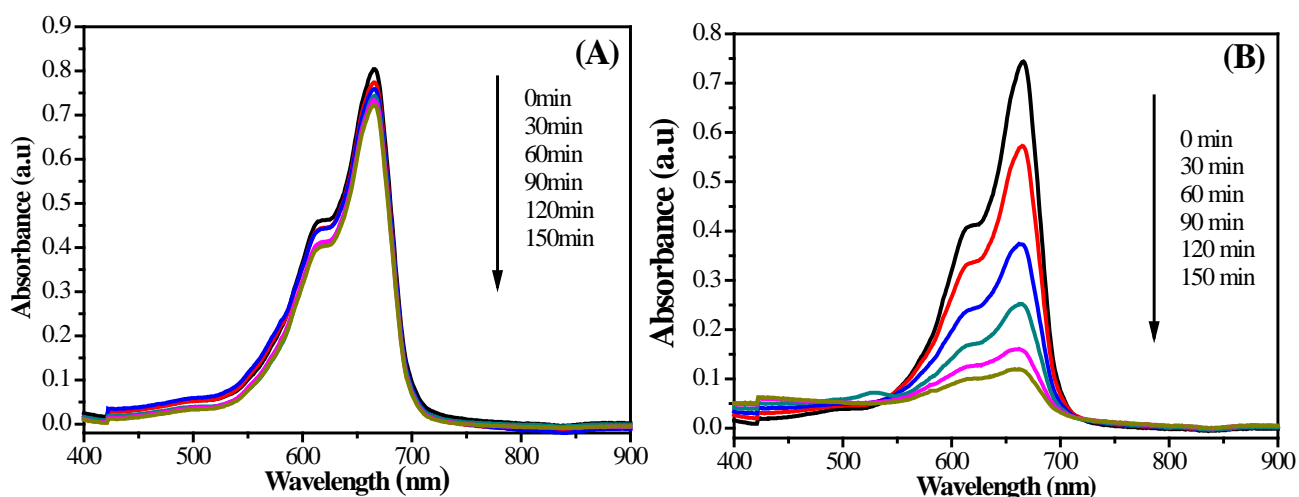


Fig. 7 Raman spectra of  $10^{-4}$  M MB solution adsorbed on (A) Ag/TiO<sub>2</sub> NTA and (B) GO/Ag/TiO<sub>2</sub> NTA with exposure treatment for (a) 0 day and (b) 60 days.

### 3.6 Self-cleaning performance of GO/Ag/TiO<sub>2</sub> NTA

The recyclability of SERS substrate is very important for practical SERS spectrum detection application. The GO/Ag/TiO<sub>2</sub> NTA showed the SERS detection limit of  $1.0 \times 10^{-9}$  M MB. The SERS activity of GO/Ag/TiO<sub>2</sub> NTA substrate was comparable and even superior to some reported Ag-based substrates<sup>28,51</sup>. Furthermore, GO/Ag/TiO<sub>2</sub> NTA substrate could achieve self-cleaning function through photocatalytic degradation of organic molecules absorbed on the surface of SERS substrate. The self-cleaning performance of GO/Ag/TiO<sub>2</sub> NTA was investigated through photocatalytic decomposition of MB molecule under solar light irradiation. A 150 W Xenon arc lamp served as a simulated solar light source. Prior to solar light irradiation, both GO/Ag/TiO<sub>2</sub> NTA and Ag/TiO<sub>2</sub> NTA were immersed in  $1.2 \times 10^{-5}$  M MB solution for 2 h in the dark to reach adsorption equilibrium. The solution samples were collected at regular intervals to analyze MB concentration during photocatalytic degradation of MB. Fig. 8(A-C) shows the UV-Vis spectra of MB during direct photolysis, Ag/TiO<sub>2</sub> NTA and GO/Ag/TiO<sub>2</sub> NTA photocatalysis processes. The Raman characteristic peak intensity at 664 nm was slightly decreased during direct photolysis process. The degradation ratio was about 10% after 150 min. Comparatively, the Raman characteristic peak almost completely disappeared after 150 min during Ag/TiO<sub>2</sub> NTA and GO/Ag/TiO<sub>2</sub> NTA photocatalysis processes. Fig. 8(D) shows the photocatalytic degradation curves of MB on the base of Ag/TiO<sub>2</sub> NTA and GO/Ag/TiO<sub>2</sub> NTA under solar light irradiation. The degradation ratio of MB was 85.3% for the Ag/TiO<sub>2</sub> NTA and 92.3% for GO/Ag/TiO<sub>2</sub> NTA. So, the GO/Ag/TiO<sub>2</sub> NTA exhibited the higher photocatalytic degradation efficiency than Ag/TiO<sub>2</sub> NTA. In general, TiO<sub>2</sub> photocatalysis degradation reaction often follows the pseudo first-order kinetic law<sup>52</sup>. The photocatalysis degradation curves is generally fitted using a Langmuir-Hinshelwood kinetic equation of  $\ln C/C_0 = kt$ , where  $C/C_0$  is the degradation ratio of MB;  $t$  is reaction time; and  $k$  is the apparent reaction-rate constant<sup>53</sup>. Accordingly, the reaction rate constant was determined to be  $0.0132 \text{ min}^{-1}$  for Ag/TiO<sub>2</sub> NTA and  $0.0165 \text{ min}^{-1}$  for GO/Ag/TiO<sub>2</sub> NTA. GO/Ag/TiO<sub>2</sub> NTA had higher photocatalysis reactivity than Ag/TiO<sub>2</sub> NTA to form a self-cleaning surface of SERS substrate. For Ag/TiO<sub>2</sub> NTA, the work function of Ag (4.26 eV) is lying below the conduction band of TiO<sub>2</sub> (4.2 eV)<sup>54</sup>, the Schottky barriers are formed between Ag NPs and TiO<sub>2</sub> NTA. As a result, the photogenerated electrons facily transfer from the conduction band of TiO<sub>2</sub> NTA to Ag NPs. For GO/Ag/TiO<sub>2</sub> NTA, both Ag NPs and GO serve as acceptors of the photogenerated electrons from TiO<sub>2</sub> NTA. Ag NPs get intimate contact with GO at the top surface of TiO<sub>2</sub> NTA. The photogenerated electrons are transferred from Ag NPs to GO. The electrons will react with surface adsorbed oxygen molecules or dissolved oxygen in water form various reactive oxidative radical species leading to the degradation of MB. The electron-accepting and transporting properties of GO and the intimate contact are formed between the GO and Ag NPs, which greatly facilitates the transfer of the photoinduced electrons<sup>55</sup>. Additionally, GO can well adsorb MB molecule and then concentrate them near the GO/Ag/TiO<sub>2</sub> NTA surface to promote the photocatalytic degradation of organic molecule.



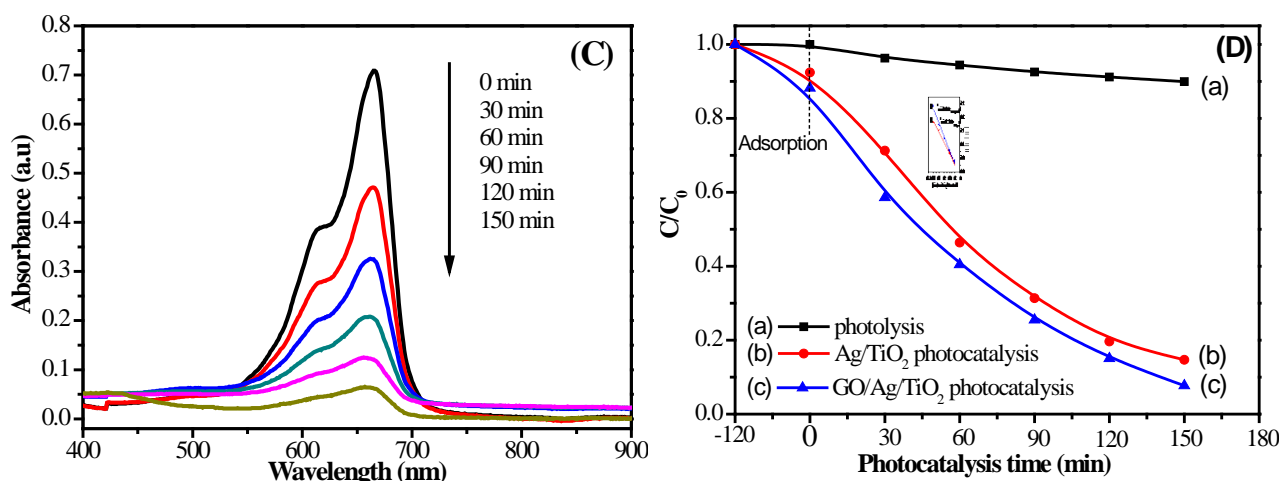


Fig. 8 UV-Vis spectra of  $1.2 \times 10^{-5}$  M MB through (A) direct photolysis, (B)  $\text{Ag}/\text{TiO}_2$  NTA photocatalysis, and (C)  $\text{GO}/\text{Ag}/\text{TiO}_2$  NTA photocatalysis under solar light irradiation; (D) Photocatalytic degradation curves of MB on the base of  $\text{Ag}/\text{TiO}_2$  NTA and  $\text{GO}/\text{Ag}/\text{TiO}_2$  NTA.

The recyclability of  $\text{GO}/\text{Ag}/\text{TiO}_2$  NTA was further investigated in SERS spectrum detection application. Briefly, the  $\text{GO}/\text{Ag}/\text{TiO}_2$  NTA was immersed in  $10^{-6}$  M MB solution for 2 h and conducted Raman spectrum measurement. This  $\text{GO}/\text{Ag}/\text{TiO}_2$  NTA substrate with adequate chemisorption of MB was immersed in distilled water and conducted photocatalysis degradation reaction for 150 min under solar light irradiation. The complete degradation of organic molecule caused to form the recovered  $\text{GO}/\text{Ag}/\text{TiO}_2$  NTA substrate, achieving a self-cleaning function. This recovered SERS substrate was applied for Raman spectrum measurement again. The above procedure was denoted as one whole recycle. SERS activity and self-cleaning performance of  $\text{GO}/\text{Ag}/\text{TiO}_2$  NTA substrate was conducted for twenty recycles. Fig. 9(A) shows SERS spectra of MB for twenty recycles through photocatalysis self-cleaning treatment of  $\text{GO}/\text{Ag}/\text{TiO}_2$  NTA. Obviously,  $\text{GO}/\text{Ag}/\text{TiO}_2$  NTA substrate with adequate chemisorption of MB had similar Raman spectrum during twenty recycling applications. Comparatively, all characteristic peaks of MB were completely disappeared in Raman spectrum after complete photocatalysis degradation of the adsorbed MB under solar light irradiation. Herein, MB molecule adsorbed on the substrate was degraded into some small molecules such as  $\text{CO}_2$  and  $\text{H}_2\text{O}$ . So, the Raman peak could be completely neglected on the self-cleaning  $\text{GO}/\text{Ag}/\text{TiO}_2$  NTA substrate. Fig. 9(B) shows Raman characteristic peak intensity before and after self-cleaning treatment. In view of the recycling SERS detection application of  $\text{GO}/\text{Ag}/\text{TiO}_2$  NTA, the Raman peak intensity of MB decreases along with the increase of recycles. However, the Raman characteristic peaks of MB could be fully observed to keep almost same intensity even after five recycles through photocatalysis self-cleaning process. The Raman spectra of MB on the recovered substrate were very similar to that on a new fresh substrate. The Raman peak intensity almost kept the similar level for the recovered  $\text{GO}/\text{Ag}/\text{TiO}_2$  NTA substrate. The Raman peak intensity of MB still kept 55% of the original intensity even after twenty recycles through photocatalysis self-cleaning process. The result revealed the good recyclability of  $\text{GO}/\text{Ag}/\text{TiO}_2$  NTA substrate. The  $\text{GO}/\text{Ag}/\text{TiO}_2$  NTA was feasible to use as a recyclable SERS substrate in the SERS detection application.

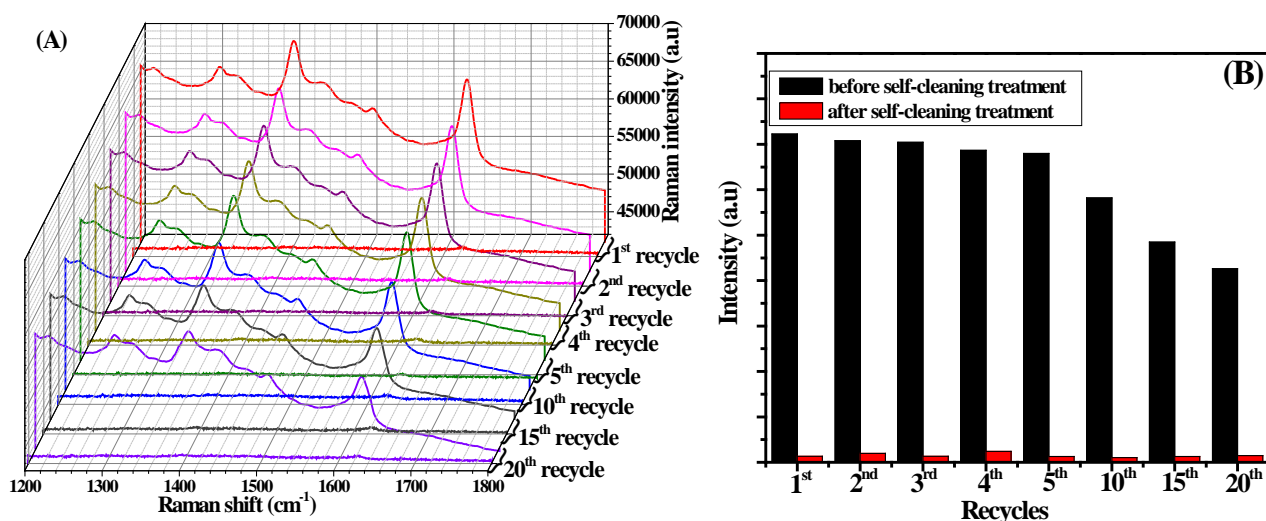


Fig. 9 (A) SERS spectra of MB for twenty recycles through photocatalysis self-cleaning treatment of GO/Ag/TiO<sub>2</sub> NTA; (B) Raman characteristic peak intensity before and after self-cleaning treatment.

### 3.7 SERS detection of BPA

Ag/TiO<sub>2</sub> NTA and GO/Ag/TiO<sub>2</sub> NTA were further applied for SERS detection of BPA, which was regarded as a typical endocrine disruptor in the environment. Fig. 10(A) shows the SERS spectra of  $5 \times 10^{-4}$  M BPA solution adsorbed on Ag/TiO<sub>2</sub> and GO/Ag/TiO<sub>2</sub> NTA. Raman characteristic peaks of BPA molecule were observed on GO/Ag/TiO<sub>2</sub> NTA. Comparatively, these characteristic peaks of BPA were not observed on Ag/TiO<sub>2</sub> NTA. The affinity of BPA molecule to Ag NPs surface was rather weak, resulting in poor SERS signals on Ag/TiO<sub>2</sub> NTA. GO was capable of adsorbing BPA molecule through  $\pi$ - $\pi$  interaction and hydrogen bond. Accordingly, BPA molecule could be accessibly trapped on GO/Ag/TiO<sub>2</sub> NTA in the Raman enhancement region and resulted in better SERS activity performance.

GO/Ag/TiO<sub>2</sub> NTA substrate was used to SERS detection of BPA with different concentration. Fig. 10(B) shows the Raman spectra of BPA with a concentration from  $5 \times 10^{-7}$  M to  $5 \times 10^{-4}$  M. SERS signals of BPA were observed and the characteristic peaks could be clearly distinguished. The Raman peaks at 638 cm<sup>-1</sup>, 822 cm<sup>-1</sup> and 1176 cm<sup>-1</sup> were assigned to phenyl ring skeletal vibration. The Raman peaks at 912 cm<sup>-1</sup> and 1110 cm<sup>-1</sup> were assigned to C-C-C asymmetric stretching vibration and =C-C bending vibration, respectively<sup>56</sup>. The Raman peaks at 1320 cm<sup>-1</sup> and 1597 cm<sup>-1</sup> were considered as the characteristic D band and G band of GO. The intensity of Raman peaks of BPA descended with the decrease of BPA concentration, whereas the intensities of the D and G bands of GO kept nearly unchanged. Such SERS signals of BPA could still be well observed even at a low concentration of  $5 \times 10^{-7}$  M. This result indicates that GO/Ag/TiO<sub>2</sub> NTA could be used for sensitive SERS detection of these organic molecules with weak affinity to Ag/TiO<sub>2</sub> NTA substrate.

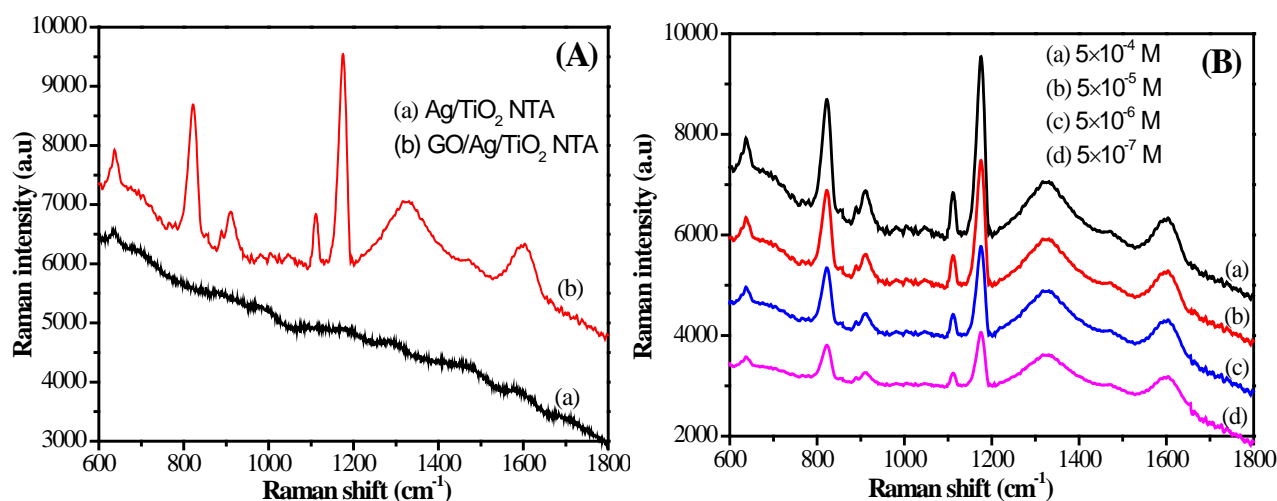


Fig. 10 (A) SERS spectra of  $5 \times 10^{-4}$  M BPA solution adsorbed on (a) Ag/TiO<sub>2</sub> NTA and (b) GO/Ag/TiO<sub>2</sub> NTA; (B) Raman spectra of BPA at different concentration of (a)  $5 \times 10^{-4}$  M, (b)  $5 \times 10^{-5}$  M, (c)  $5 \times 10^{-6}$  M and (d)  $5 \times 10^{-7}$  M adsorbed on GO/Ag/TiO<sub>2</sub> NTA.

#### 4. Conclusions

Graphene oxide decorated silver nanoparticles/titania nanotube array had been designed as SERS substrate for SERS detection of organic molecules. Well-aligned TiO<sub>2</sub> NTA was fabricated by a controlled anodic oxidation process. Ag/TiO<sub>2</sub> NTA was prepared by uniformly depositing Ag NPs on the surface of anatase TiO<sub>2</sub> NTA via a polyol process. GO/Ag/TiO<sub>2</sub> NTA were obtained by decorating GO on the surface of Ag/TiO<sub>2</sub> NTA through an impregnation method. The GO/Ag/TiO<sub>2</sub> NTA exhibited adsorption ratio of 38.0% MB, AEF of  $3.67 \times 10^4$  and a detection limit of  $1.0 \times 10^{-9}$  M, presenting good adsorption capability and high sensitivity for SERS detection of MB. The GO/Ag/TiO<sub>2</sub> NTA was used for SERS detection of BPA with a weak affinity, achieving good adsorption capability of 23.8% BPA and a detection limit as low as  $5 \times 10^{-7}$  M. Furthermore, the GO/Ag/TiO<sub>2</sub> NTA substrate could achieve self-cleaning function through photocatalytic degradation of organic molecules absorbed on the surface of SERS substrate under solar light irradiation. GO/Ag/TiO<sub>2</sub> NTA shows higher adsorption capability and better SERS performance than Ag/TiO<sub>2</sub> NTA. Therefore, the sensitive and recyclable GO/Ag/TiO<sub>2</sub> NTA substrate presented the promising application for SERS detection of diversified organic molecules.

#### Acknowledgement

The work was supported by National Natural Science Foundation of China (No. 21373047 and 20871029), Program for New Century Excellent Talents in University of the State Ministry of Education (No. NCET-08-0119), Science & Technology Program of Suzhou City (No. ZXG2012026, SYN201208, SYG201017).

## Notes and References

1. M. K. Fan, G. F. S. Andrade and A. G. Brolo, *Anal. Chim. Acta*, 2011, **693**, 7-25.
2. R. A. Halvorson and P. J. Vikesland, *Environ. Sci. Technol.*, 2010, **44**, 7749-7755.
3. S. Shanmukh, L. Jones, J. Driskell, Y. P. Zhao, R. Dluhy and R. A. Tripp, *Nano Lett.*, 2006, **6**, 2630-2636.
4. J. R. Lombardi and R. L. Birke, *J. Phys. Chem. C*, 2008, **112**, 5605-5617.
5. B. L. Sun, X. H. Jiang, S. X. Dai and Z. L. Du, *Mater. Lett.*, 2009, **63**, 2570-2573.
6. Y. D. Wang, N. Lu, W. T. Wang, L. X. Liu, L. Feng, Z. F. Zeng, H. B. Li, W. Q. Xu, Z. J. Wu, W. Hu, Y. Q. Lu and L. F. Chi, *Nano Res.*, 2013, **6**, 159-166.
7. X. H. Li, G. Y. Chen, L. B. Yang, Z. Jin and J. H. Liu, *Adv. Funct. Mater.*, 2010, **20**, 2815-2824.
8. H. Y. Chu, Y. J. Liu, Y. W. Huang and Y. P. Zhao, *Opt. Express*, 2007, **15**, 12230-12239.
9. R. Zhang, M. Hummelgård and H. Olin, *PLoS One*, 2012, **7**, e30469.
10. X. Liu, B. Choi, N. Gozubenli and P. Jiang, *J. Colloid Interface Sci.*, 2013, **409**, 52-58.
11. P. Pinkhasova, H. Chen, M. W. G. M. Verhoeven, S. Sukhishvili and H. Du, *RSC Adv.*, 2013, **3**, 17954-17961.
12. W. Wang, Y. Xie, Y. Wang, H. Du, C. Xia and F. Tian, *Microchim. Acta*, 2014, **181**, 381-387.
13. Y. Xie, Y. Wang and H. Du, *Mater. Sci. Eng., B*, 2013, **178**, 1443-1451.
14. Y. Xie and Y. Zhao, *Mater. Sci. Eng., C*, 2013, **33**, 5028-5035.
15. Y. Xie and X. Fang, *Electrochim. Acta*, 2014, **120**, 273-283.
16. H. Du, Y. Xie, C. Xia, W. Wang and F. Tian, *New J. Chem.*, 2014, **38**, 1284-1293.
17. H. Du, Y. Xie, C. Xia, W. Wang, F. Tian and Y. Zhou, *Mater. Lett.*, 2014, **132**, 417-420.
18. W. Wang, Y. Xie, C. Xia, H. Du and F. Tian, *Microchim. Acta*, 2014, **181**, 1325-1331.
19. C. Xia, Y. Xie, Y. Wang, W. Wang, H. Du and F. Tian, *J. Appl. Electrochem.*, 2013, **43**, 1225-1233.
20. C. Xia, Y. Xie, W. Wang and H. Du, *Synth. Met.*, 2014, **192**, 93-100.
21. A. Musumeci, D. Gosztola, T. Schiller, N. M. Dimitrijevic, V. Mujica, D. Martin and T. Rajh, *J. Am. Chem. Soc.*, 2009, **131**, 6040-6041.
22. Y. Li, T. Sasaki, Y. Shimizu and N. Koshizaki, *J. Am. Chem. Soc.*, 2008, **130**, 14755-14762.
23. Y. Xie, Y. Jin, Y. Zhou and Y. Wang, *Appl. Surf. Sci.*, 2014, **133**, 549-557.
24. Y. J. Chen, G. H. Tian, K. Pan, C. G. Tian, J. Zhou, W. Zhou, Z. Y. Ren and H. G. Fu, *Dalton Trans.*, 2012, **41**, 1020-1026.
25. X. J. Liu, L. Y. Cao, W. Song, K. L. Ai and L. H. Lu, *Acs Appl. Mater. Interface*, 2011, **3**, 2944-2952.
26. Z. M. Liu, H. Q. Zhong, Z. Y. Guo and B. W. Yang, *Chin. Opt. Lett.*, 2013, **11**.
27. X. Ling, L. M. Xie, Y. Fang, H. Xu, H. L. Zhang, J. Kong, M. S. Dresselhaus, J. Zhang and Z. F. Liu, *Nano Lett.*, 2010, **10**, 553-561.
28. W. Fan, Y. H. Lee, S. Pedireddy, Q. Zhang, T. X. Liu and X. Y. Ling, *Nanoscale*, 2014, **6**, 4843-4851.
29. G. Lu, H. Li, C. Liusman, Z. Y. Yin, S. X. Wu and H. Zhang, *Chem. Sci.*, 2011, **2**, 1817-1821.
30. L. Tzounis, R. Contreras-Caceres, L. Schellkopf, D. Jehnichen, D. Fischer, C. Cai, P. Uhlmann and M. Stamm, *RSC Adv.*, 2014, **4**, 17846-17855.
31. Y. Q. Liang, Z. D. Cui, S. L. Zhu, Y. Liu and X. J. Yang, *J. Catal.*, 2011, **278**, 276-287.
32. P. Song, X. Y. Zhang, M. X. Sun, X. L. Cui and Y. H. Lin, *Nanoscale*, 2012, **4**, 1800-1804.
33. W. S. Hummers and R. E. Offeman, *J. Am. Chem. Soc.*, 1958, **80**, 1339-1339.
34. T. Ohsaka, F. Izumi and Y. Fujiki, *J. Raman Spectrosc.*, 1978, **7**, 321-324.
35. C. Chen, W. M. Cai, M. C. Long, B. X. Zhou, Y. H. Wu, D. Y. Wu and Y. J. Feng, *Acs Nano*, 2010, **4**, 6425-6432.
36. D. Graf, F. Molitor, K. Ensslin, C. Stampfer, A. Jungen, C. Hierold and L. Wirtz, *Nano Lett.*, 2007, **7**, 238-242.
37. M. C. Long, Y. L. Qin, C. Chen, X. Y. Guo, B. H. Tan and W. M. Cai, *J. Phys. Chem. C*, 2013, **117**, 16734-16741.
38. X. G. M. Shiqing, *Chem. Phys. Lett.*, 2007, **447**, 305-309.
39. G. K. Ramesha, A. V. Kumara, H. B. Muralidhara and S. Sampath, *J. Colloid Interface Sci.*, 2011, **361**, 270-277.
40. J. Balapanuru, J. X. Yang, S. Xiao, Q. L. Bao, M. Jahan, L. Polavarapu, J. Wei, Q. H. Xu and K. P. Loh, *Angew. Chem.-Int. Edit.*, 2010, **49**, 6549-6553.

41. Y. Wang, Y. H. Tang, Y. Chen, Y. Li, X. N. Liu, S. L. Luo and C. B. Liu, *J. Mater. Sci.*, 2013, **48**, 6203-6211.
42. J. Xu, L. Wang and Y. F. Zhu, *Langmuir*, 2012, **28**, 8418-8425.
43. S. Pal, L. E. Depero and I. Alessandri, *Nanotechnology*, 2010, **21**.
44. Q. Z. Hao, B. Wang, J. A. Bossard, B. Kiraly, Y. Zeng, I. K. Chiang, L. Jensen, D. H. Werner and T. J. Huang, *J. Phys. Chem. C*, 2012, **116**, 7249-7254.
45. J. F. Li, Y. F. Huang, Y. Ding, Z. L. Yang, S. B. Li, X. S. Zhou, F. R. Fan, W. Zhang, Z. Y. Zhou, D. Y. Wu, B. Ren, Z. L. Wang and Z. Q. Tian, *Nature*, 2010, **464**, 392-395.
46. X. X. Yu, H. B. Cai, W. H. Zhang, X. J. Li, N. Pan, Y. Luo, X. P. Wang and J. G. Hou, *Acs Nano*, 2011, **5**, 952-958.
47. E. C. Le Ru, E. Blackie, M. Meyer and P. G. Etchegoin, *J. Phys. Chem. C*, 2007, **111**, 13794-13803.
48. Y. M. Liu, Y. Hu and J. Zhang, *J. Phys. Chem. C*, 2014, **118**, 8993-8998.
49. G. M. H. Goncher, C. B., *J. Chem. Phys.*, 1982, **77**, 3767-3768.
50. Y. D. Zhao, Y. Z. Xie, Z. Y. Bao, Y. H. Tsang, L. M. Xie and Y. Chai, *J. Phys. Chem. C*, 2014, **118**, 11827-11832.
51. Y. Yang, Z. Y. Li, K. Yamaguchi, M. Tanemura, Z. R. Huang, D. L. Jiang, Y. H. Chen, F. Zhou and M. Nogami, *Nanoscale*, 2012, **4**, 2663-2669.
52. Y. Xie and D. Fu, *Mater. Res. Bull.*, 2010, **45**, 628-635.
53. S. Y. Kim, T. H. Lim, T. S. Chang and C. H. Shin, *Catal. Lett.*, 2007, **117**, 112-118.
54. M. H.B., *J.Appl.Phys*, 1977, **48**, 4729-4733.
55. S. X. Min and G. X. Lu, *J. Phys. Chem. C*, 2011, **115**, 13938-13945.
56. S. T. Wang, H. Z. Lu, N. Ma, Y. Bao, H. Y. Wang, Z. G. Liu and W. R. Yao, *Spectrosc. Spect. Anal.*, 2011, **31**, 1006-1009.